Numerical analysis of the hydrodynamic loading of a floating tidal turbine undergoing the pendulum motion

Mohamad Hasif Osman[1,*], Richard Willden[1]

(1. *Department of Engineering Science, University of Oxford, Oxford, UK*)

Abstract: For a floating offshore turbine freely oscillate in the six degrees of freedom motion, the origin of the unsteady loading comes from the combination of tidal current, waves, and the platform (and turbine) motion. In literature, the pendulum (pitch) motion is viewed as the dominant contributor, in terms of the wave-induced platform motion, to the fluctuating load on a floating turbine. This paper aims to analyze the unsteady hydrodynamic loading on the floating tidal turbine oscillating in the pendulum motion. Computational fluid dynamics (CFD) analyses were carried out to investigate the performance of the floating turbine. The fluctuating load was highly in phase with the instantaneous velocity on the rotor. Loading variations increase together with the increase in motion amplitude and frequency. Flow separation occurs at higher motion amplitude and frequency cases, which is detrimental to the structural integrity of the rotor. Implementing the speed control technique by spinning the rotor faster can minimize the stalling effect on the floating turbine. The research finding can provide useful insight into understanding the unsteady loading on a floating tidal turbine oscillating in the pendulum motion.

Keywords: pitch motion, tidal turbine, stall, floating, unsteady loading, OpenFOAM

* Corresponding author.

Email address: mhasif02@gmail.com (M. Osman)

Department of Engineering Science, University of Oxford, Oxford, UK

Numerical analysis of the hydrodynamic loading of a floating tidal turbine undergoing the pendulum motion

Mohamad Hasif Osman[1,*], Richard Willden[1]

(1. *Department of Engineering Science, University of Oxford, Oxford, UK*)

Abstract: For a floating offshore turbine freely oscillate in the six degrees of freedom motion, the origin of the unsteady loading comes from the combination of tidal current, waves, and the platform (and turbine) motion. In literature, the pendulum (pitch) motion is viewed as the dominant contributor, in terms of the wave-induced platform motion, to the fluctuating load on a floating turbine. This paper aims to analyze the unsteady hydrodynamic loading on the floating tidal turbine oscillating in the pendulum motion. Computational fluid dynamics (CFD) analyses were carried out to investigate the performance of the floating turbine. The fluctuating load was highly in phase with the instantaneous velocity on the rotor. Loading variations increase together with the increase in motion amplitude and frequency. Flow separation occurs at higher motion amplitude and frequency cases, which is detrimental to the structural integrity of the rotor. Implementing the speed control technique by spinning the rotor faster can minimize the stalling effect on the floating turbine. The research finding can provide useful insight into understanding the unsteady loading on a floating tidal turbine oscillating in the pendulum motion.

Keywords: pitch motion, tidal turbine, stall, floating, unsteady loading, OpenFOAM

* Corresponding author.

Email address: mhasif02@gmail.com (M. Osman)

Department of Engineering Science, University of Oxford, Oxford, UK

1. Introduction

The wind energy community has extensively studied the dynamics of floating offshore wind turbines, ranging from individual floating rotors to wind farms (Wen et al., 2017; Micallef & Sant, 2015; Castro-Santos & Diaz-Casas, 2015; Rodrigues et al., 2015). Some focus on an individual degree of freedom (DoF) motion, while others looked at a fully coupled model with 6 DoF oscillations (Tran & Kim, 2015a; Jonkman, 2009). Even though the mechanics behind wind and tidal turbines are similar, the key difference between the two is the higher loading experienced by tidal turbines due to a much higher fluid density and the blockage effect which

is not as significant in wind turbine operations (Schluntz & Willden, 2015; Wimshurst & Willden, 2016).

Although tidal energy has been around for more than a decade, not many have researched floating tidal turbines. Studies such as by Jing et al. (2017), Osman et al. (2020) and Brown et al. (2020) focus more on a single degree of freedom (DoF) to evaluate the unsteady loading on the floating tidal turbine. Others concentrate on multi-DoF motion through experiments and numerical simulations (Xie et al., 2019; Brown et al., 2021). One of the main interests of the present study is to focus on a single DoF motion of a floating tidal turbine to investigate the dynamics of the unsteady loading of the rotor. Brown et al. (2020) conducted a numerical study on floating tidal turbines under wave conditions using an actuator disc model. They found that pitch motion has the most influence on the unsteady loading on the turbine. Others also found that the pitch motion is the most significant in contributing to the unsteady (fluctuating) loading of a floating turbine found in the literature (Bagbanci, 2011; Sebastian & Lackner, 2012; Pegalajar-Jurado et al., 2016). Therefore, the pitch motion will be discussed in this paper. In the present study, the term 'pendulum' will be used instead of 'pitch' in describing the motion since, in the present study, the former better represents the motion than the latter.

Investigating the effects of motion amplitude and frequency on the floating turbine performance is crucial in understanding the mechanics behind the unsteady forces (Lienard et al., 2019). For example, the fluctuating load on a floating turbine is highly in phase with the instantaneous velocity on the rotor, which affects the device's performance. In a high instantaneous velocity (i.e., apparent velocity) condition, which happens in high motion amplitude and frequency cases, the loading will increase and in some cases, they might go into stall. A turbine will go into stall when the flow separates from the surface of the rotor blade due to the increase in the angle of attack (Osman et al., 2020; Osman & Willden, 2021). The stalling effect is also recorded in the findings of Lienard et al. (2019) for the higher motion amplitude case. The stalling effect promotes fatigue damage on rotor blades, which can reduce the design life of the device, and also minimise the power production of the turbine due to the loss in lifts from flow separation (Osman et al., 2020). Therefore, this phenomenon will be addressed in this paper together with the potential way to overcome this problem.

2. Numerical method

The diagram of the computational domain is given in Figure 1. An in-house blocked rotor design from Wimshurst & Willden (2016) was used in the present study. It is a three-bladed rotor designed using the RISØ-A1-24 aerofoil with a size of 20 m in diameter *D*. This rotor design was chosen for the present study because of its thicker blade design which is more realistic for a tidal turbine operating under a harsh oceanic environment. Further detail on the rotor design can be found in Wimshurst & Willden (2016). The rotor is offset *a"* = 0.4*D* from the centre of rotation (COR), which is from the in-house design concept of a floating tidal turbine presented in Osman & Willden (2020). The nacelle centreline is located 1*D* below the COR. The oscillating rotating motion function, a rigid body motion function which is readily available in OpenFOAM, is applied to the middle and inner domain meshes using the sliding mesh method to simulate the pendulum motion of the turbine about the COR. For the inner domain mesh, another function, which is the rotating motion function, is applied using the multi solid body motion function, which is also available in OpenFOAM. For the present study, the blockage ratio B = 0.01; this is to eliminate the effect of the blockage ratio on the turbine performance since only the effect of the pendulum motion is of interest.

In the wind and tidal energy industry, power and thrust coefficients are widely used to measure a turbine's performance. The power coefficient is defined as the ratio of power extracted by the turbine, P_D, over the total available power, P_T, in the flow (Burton et al. 2001),

$$C_P = \frac{P_D}{P_T} = \frac{Q.\omega_r}{\frac{1}{2}\rho U_\infty^3 A_D} \qquad (1)$$

where ρ is the fluid density, U_∞ is the free stream velocity, Q is the rotor torque, ω_r is the rotor rotational speed, and A_D is the swept area of the rotor. The thrust coefficient can be defined as

$$C_T = \frac{T}{\frac{1}{2}\rho U_\infty^2 A_D} \qquad (2)$$

where T is the rotor thrust. These definitions can only be used for a non-oscillating turbine (for example, a bottom fixed tidal turbine). For a floating turbine, the instantaneous velocity varies over time since it constantly oscillates in six degrees of freedom (DoF). Therefore, the apparent velocity $U_{ap}(t)$ can be used instead of U_∞ to define P_D, P_T and T. By substituting U_{ap} into U_∞ in equations 1 and 2, a new definition can be established, called the power and thrust efficiencies, η_P and η_T respectively.

$$\eta_P = \frac{P_D(t)}{\frac{1}{2}\rho U_{ap}(t)^3 A_D} \qquad (3a)$$

$$\eta_T = \frac{T(t)}{\frac{1}{2}\rho U_{ap}(t)^2 A_D} \qquad (3b)$$

where $T(t)$ and $P_D(t)$ are, respectively, the time-varying thrust and power extracted by a floating turbine undergoing prescribed motions.

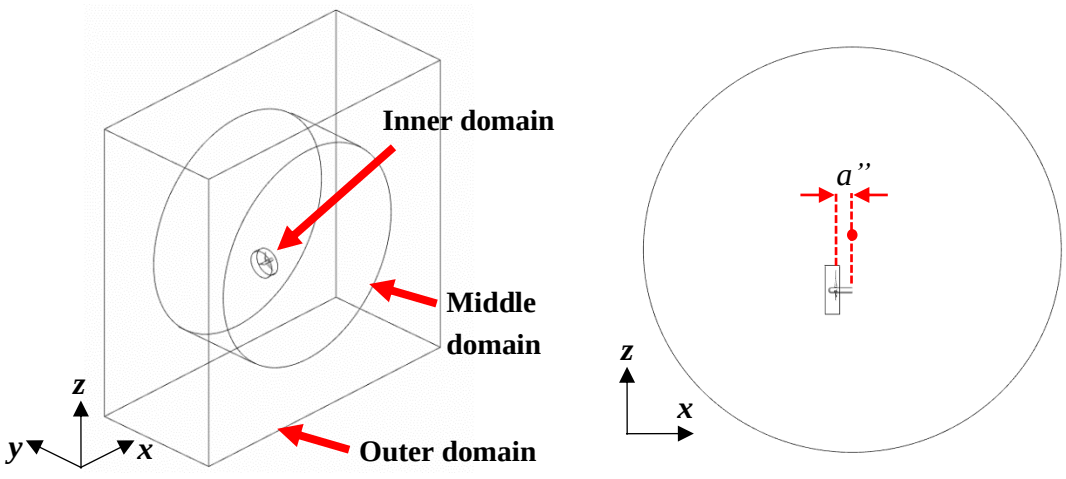

(a) Computational domain (b) Side view

Figure 1 Diagrams of (a) the computational domain and (b) the side view of the domain, showing the offset *a''* of the turbine plane from the COR.

For a floating turbine oscillating under prescribed pendulum motion, the rotor's instantaneous angular motion about the centre of rotation (COR) is defined as

$$\theta_{\text{pen}}(t) = -A_0 \sin(\omega_0 t) \qquad (4)$$

where A_0 and ω_0 are motion amplitude (m) and angular frequency (rad/s), respectively. The relationship between the angular displacement, apparent velocity, and the motion velocity is presented in Figure 2 for a floating turbine oscillating at an amplitude $A_0 = 1.5°$ and frequency $\omega^* = \omega_0/\omega_r = 1.0$. The rotational displacement is negative as the turbine swings upstream and positive as it retreats downstream. The apparent velocity U_{ap}, which is the flow velocity relative to the rotor, is 90° out of phase with the turbine's rotational displacement, such that the maximum U_{ap} occur as the turbine moves into its original position from downstream to upstream and *vice versa* for minimum U_{ap}. Based on Lienard et al. (2019), the apparent velocity can be calculated as

$$U_{ap}(t) = U_\infty \cos\theta_{pen}(t) - \dot{\theta}_{\text{pen}}(t).h \qquad (5)$$

where $\dot{\theta}_{\text{pen}}$ is the rotor pendulum velocity (rad/s), and h = 20 m is the rotational arm length from the centreline of the turbine nacelle to the centre of rotation. The $k-\omega$ SST turbulence model by Menter (1994) was used in the present study. The velocity inlet boundary condition was applied at the inlet with a constant U_∞ = 2 m/s, pressure outlet was applied at the outlet boundary, slip boundary was used on the sides of the outer domain to simulate a uniform flow, and the cyclic arbitrary mesh interface (AMI) was used at interfaces between each domain.

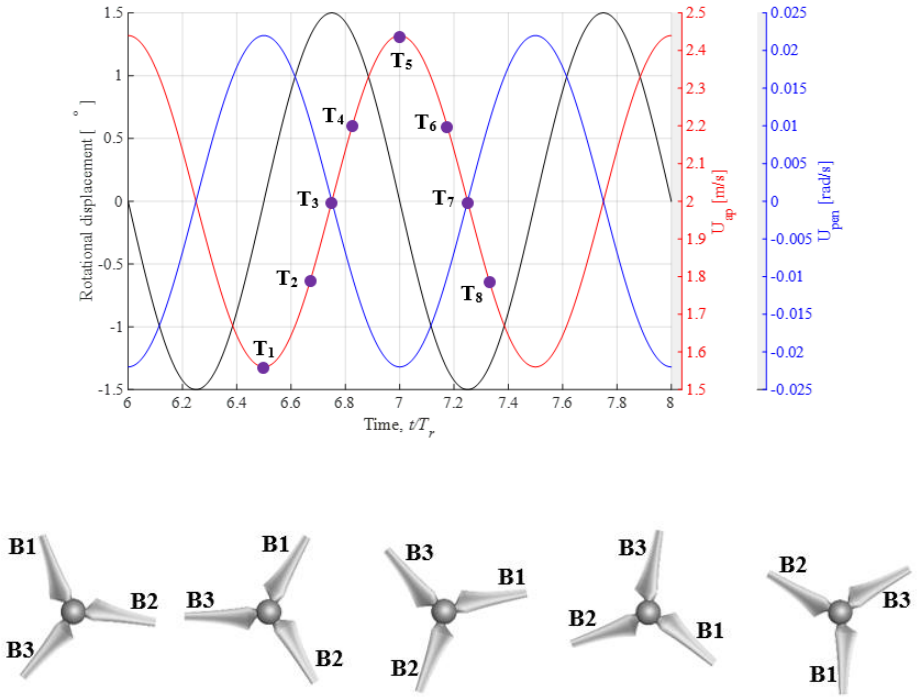

(a) T5 (b) T6 (c) T7 (d) T8 (e) T1

Figure 2 Rotational displacements, apparent velocity, and angular velocity of the pendulum motion for the case of A_0 = 1.5° with ω^* = 1.0 and λ = 4.2. The negative sign of rotational displacement shows the rotor moves forward and *vice versa* for the positive sign. The bottom figures show the azimuth position of each rotor blade at different time steps.

3. Effects of motion amplitude and frequency on turbine performance

To highlight the effect of pendulum motion on floating turbine performance, a series of tests were conducted using various motion amplitude A_0 and frequency ω^*. Based on a realistic assumption of a 20 m diameter floating turbine weighing around 1.5 tonnes (SIMEC Atlantis

Energy, 2016), five pendulum motion amplitudes, $A_0 = 1.0°, 1.5°, 2.0°, 3.0°, 4.3°$ were chosen in the present study. The motion frequency is chosen based on the wave frequency at the Fall of Warness tidal site (Anatec Ltd., 2010), with the frequency range $\omega^* = 0.6, 0.7, 0.8, 1.0, 1.3$. The rotor rotational speed $\omega_r = 0.82$ rad/s, which corresponds to the optimal tip speed ratio $\lambda = 4.2$ for this turbine design for a non-oscillating (stationary) condition at $B = 0.01$ as shown in Wimshurst & Willden (2016), is kept constant for all cases unless otherwise specified

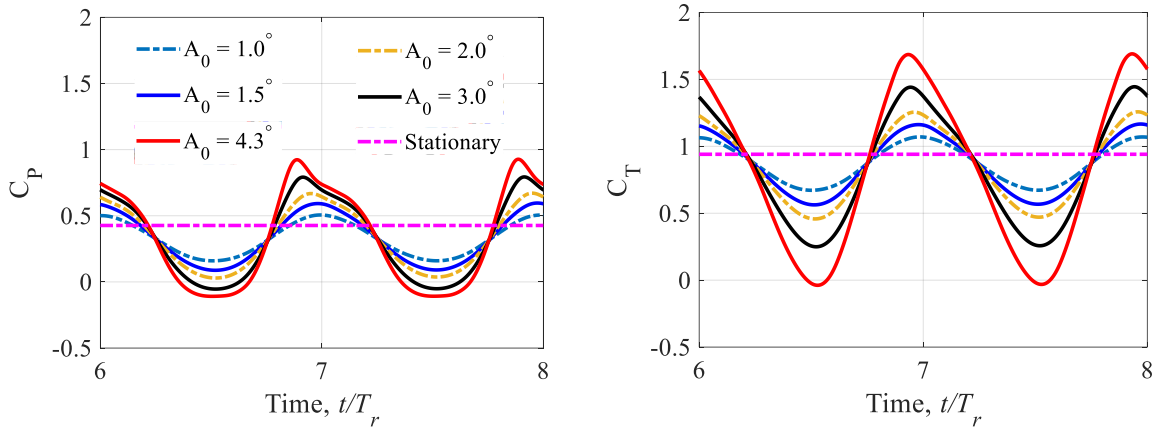

(a)

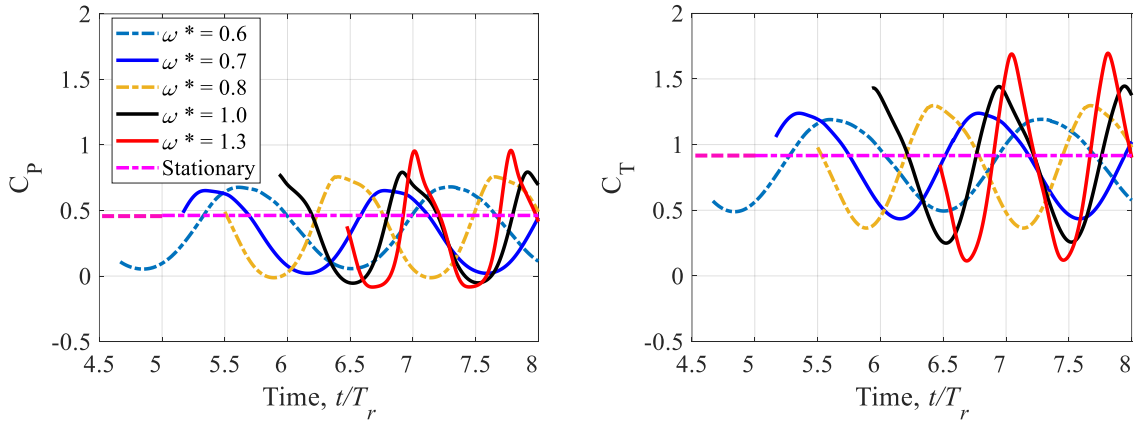

(b)

Figure 3 Time histories of power and thrust coefficients for a floating turbine undergoing a prescribed pendulum motion (a) at various motion amplitudes with a constant $\omega^* = 1.0$; and (b) at various motion frequencies with a constant $A_0 = 3°$. T_r is the period (in second) of one rotor revolution. All cases have a constant rotor rotational speed $\omega_r = 0.82$ rad/s. The pink dashed line shows the stationary power and thrust coefficients in all of the figures.

Figure 3 shows the time histories of C_P and C_T of a floating turbine undergoing pendulum motions over a range of motion amplitudes and frequencies. Note that for the various amplitude cases, the motion frequency is kept constant while for the various frequencies, the motion

amplitude remains unchanged. Simulations were carried out for ~8 rotor revolutions, and only data from the last two motion cycles were considered in the present study to ensure consistency and to eliminate the early data discrepancies of transient simulations. The amplitude of loading variation increases as the motion amplitude and frequency are increased. This is a typical loading trend for a floating turbine undergoing pendulum motion where the increase in loading amplitude is due to the increase in the instantaneous velocity of the rotor (Tran & Kim, 2015; Wen et al., 2019).

Table 1 Mean power and thrust coefficients for a floating turbine undergoing a prescribed pendulum motion over a range of motion amplitude and frequency with a constant ω_r = 8.2 rad/s. For the stationary case, the rotor rotational speed is also ω_r = 8.2 rad/s (which corresponds to λ = 4.2).

A_0 [°]	ω^*	$\bar{C}_P$	$\bar{C}_T$	Percentage difference $\bar{C}_P$ [%]	Percentage difference $\bar{C}_T$ [%]
1.0	1.0	0.331	0.875	28.5	4.6
1.5	1.0	0.337	0.872	27.2	4.9
2.0	1.0	0.342	0.867	26.1	5.5
3.0	1.0	0.344	0.853	25.7	7.0
4.3	1.0	0.347	0.836	25.1	8.8
3.0	0.6	0.364	0.858	21.4	6.4
3.0	0.7	0.334	0.854	27.9	6.9
3.0	0.8	0.365	0.846	21.2	7.7
3.0	1.0	0.344	0.853	25.7	7.0
3.0	1.3	0.320	0.818	30.8	10.8
Stationary		0.463	0.917	-	-

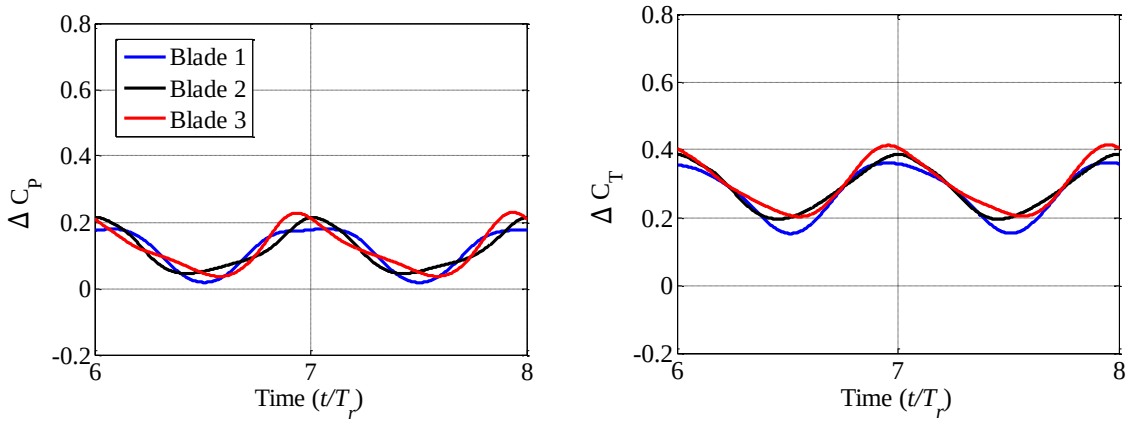

(a) A_0 = 1.5° ω^* = 1.0

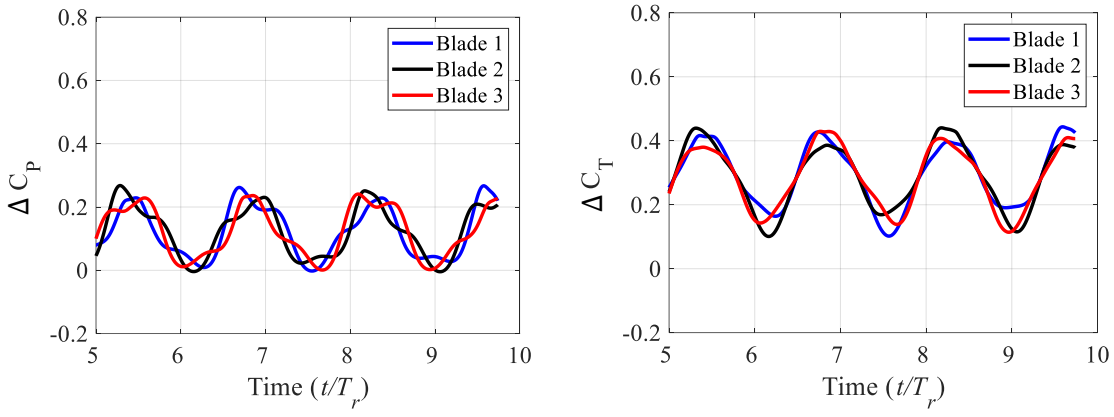

(b) A_0 = 3.0° ω^* = 0.7

Figure 4 Power and thrust coefficients for each blade, ΔC_P and ΔC_T, respectively, for a floating turbine undergoing a prescribed pendulum motion with a constant λ = 4.2. Figure (b) was purposely plot over a wider range of time to highlight the loading variation.

Besides that, higher motion amplitude increases the mean C_P and decreases mean C_T, as presented in Table 1. A similar trend is shown in the literature by Leble & Barakos (2016) and Lienard et al. (2019) for a floating wind turbine undergoing a prescribed pendulum motion. However, higher motion frequency decreases both mean C_P and C_T. This happens due to the stalling effect, where the flow starts to separate causing the loss in lifts along rotor blades due to the increase in the motion frequency. The overall mean loading values of the pendulum motion diverges from the stationary case, with mean C_P diverges more than mean C_T. This happens due to the stalling phenomenon which occurs more toward the tangential or rotating component of the load (i.e. torque) than the axial component (i.e. thrust). The stalling effect

will be discussed in the following chapter. Besides that, the reduction in mean thrust and power is due to less optimal rotor operation due to the hydrodynamic effects associated with oscillating inflow. This will be explained later when discussing the rotor's efficiency.

Looking at loading time histories on individual blades presented in Figure 4, each blade shows different loading variations and is slightly out of phase with one another. A similar trend has been shown in the literature for a floating wind turbine undergoing pendulum motion (T. Tran et al., 2014; Shen et al., 2018; Lienard et al., 2019). For the case of A_0 = 1.5°, blade 1 shows the lowest power and thrust at both minimum and maximum apparent velocities. This is because at maximum apparent velocity, blade 1 is located at its original position with azimuth angle = 0° (refer to Figure 2 for blades azimuth position). Due to the pendulum motion, the instantaneous velocity is larger at the bottom half of the rotor (blades 2 and 3) than the upper half (blade 1) when the rotor moves forward. The opposite will happen when the rotor swings backwards in the pendulum motion. Note that at minimum U_{ap} the rotor plane is at its original position with the azimuth angle of blade 1 at 180°. Although not shown here, similar behaviour can be observed in all A_0 cases with constant ω^* = 1.0. For the case of ω^* = 0.7 the loading on each blade shows variation at each motion cycle, where the maximum and minimum loading occurs on different blades at every peak and through. Blade 3 shows the lowest thrust at t/T_r = 5.4 (the first maximum apparent velocity) while at t/T_r = 6.8 (the second maximum apparent velocity) blade 3 shows the highest. The other two blades also show different variations at each cycle. This variation is due to the different azimuth angles of each blade at each maximum U_{ap}, which happens because the angular velocity of the rotor (rotor rotational speed) differs from that of the pendulum motion. When both parameters have the same value, only one blade will constantly experience the highest loading at maximum U_{ap} and one blade will constantly experience the lowest loading at minimum U_{ap}. In the present study, blade 3 is always maximum and blade 1 is always minimum at maximum (t/Tr = 7) and minimum (t/Tr = 6.5) U_{ap}, respectively, as shown in Figure 4a. In the study of a dynamic yawing wind turbine by Tran & Kim (2015), they found that in the case of rotor rotational speed equal to the motion frequency, one blade (in the present study, blade 3) is always experiencing an advancing phase while another blade (blade 1 in the present study) the retreating phase.

The power and thrust efficiencies for a turbine undergoing a prescribed pendulum motion are presented in Figure 5a. It is observed that the turbine efficiencies go to the maximum twice per motion cycle. This happens because when the rotor moves into the farthest upstream and

downstream, the value of apparent velocity is (almost) similar to the free stream velocity $(U_{ap} \approx U_{\infty})$. In this condition, the turbine operates at its optimum tip speed ratio (i.e., optimum operating condition). To describe the rotor efficiency at different apparent velocity conditions, an aerofoil sketch is presented in Figure 5b, corresponding to the markers T_1 (minimum U_{ap}, blue dashed arrows), T_5 (maximum U_{ap}, red dashed arrows), T_3 and T_7 ($U_{ap} \approx U_{\infty}$, black solid arrows). The reader can refer to Figure 2 for markers T_1 to T_7. Although, this analysis does not consider the effects of the angle of attack on the blades relative to the position of the rotor. The instantaneous flow velocity is slightly rotated (in the y-axis) at positions T_3 and T_7 due to the tilted position at farthest downstream and upstream, respectively. This will affect the angle of the free stream flow on the rotor plane, affecting the angle of attack on each blade.

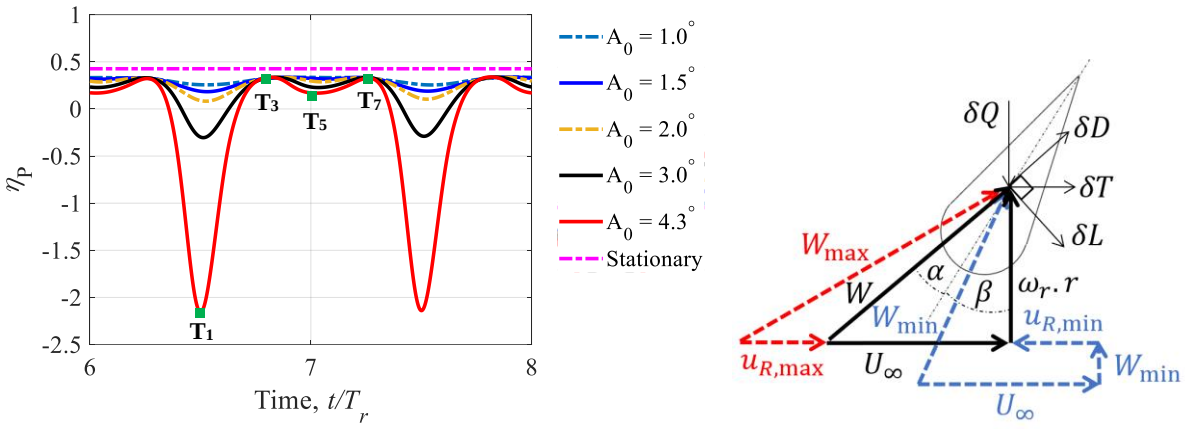

(a) (b)

Figure 5 (a) Power efficiency for a floating turbine undergoing a prescribed pendulum motion at various motion amplitudes moving at a constant ω^* = 1.0 and λ = 4.2; (b) Sketch of a blade cross-section and the flow diagram of the rotor corresponds to figure (a), where T_1 and T_5 are at the minimum and maximum apparent velocity, drawn in blue and red dashed arrow lines, respectively, and black solid arrow lines for T_3 and T_7. u_R is the additional velocity caused by the rotor's motion.

4. Stalling effects of a floating tidal turbine

In the previous chapter, we encounter many instances of stalling effects, particularly involving the flow separation along rotor blades due to the increase in the instantaneous velocity. In this chapter, we will dive further into the effects of stall on the floating turbine performance.

Previously, we come across the asymmetry at the peak of each cycle shown in the time histories plot given in Figure 3 for higher motion amplitude and frequency cases (for instance, at maximum U_{ap} at timesteps $t/T_r = 6, 7, 8$ in Figure 3a). This characteristic is more prominent in C_P than C_T. A similar trend can also be observed in the individual blade loading given in Figure 4b. This characteristic is an indication of stalling. The rotor goes into stall as the instantaneous apparent velocity U_{ap} goes to the maximum. To explain this phenomenon, we can view the axial and tangential aerodynamic force coefficients, C_X and C_Y respectively, as having components of lift and drag coefficients (C_L and C_D, respectively):

$$C_L \cos\phi + C_D \sin\phi = C_X \qquad (6a)$$

$$C_L \sin\phi - C_D \cos\phi = C_Y \qquad (6b)$$

where $\phi = \alpha + \beta$ is the resultant flow angle, α is the angle of attack and β is the blade twist angle. In the above equations, C_X can be used to derive the thrust and C_Y the torque, hence power. Now imagine a typical lift and drag over angles of attack curves of a 2-dimensional aerofoil. As U_{ap} is increased, α will also increase, and it will continue increasing until it passes the static stall angle at maximum U_{ap}. When this happens, the lift will drop, but the drag will continue to increase. Therefore, the drag is more dominant than the lift at a higher U_{ap}. This causes the power to drop considerably more than the thrust. The effect of flow separation at high U_{ap} can also be seen along each blade where the change in the characteristic of the loading (a sudden drop in loading around 80 per cent of the spanwise distance along the blade) is prominent compared to the stationary turbine, as shown in Figure 6. Figure 6 shows the force profiles along each blade of a rotor undergoing a pendulum motion at A_0 = 3.0° and ω^* = 1.0 at different time step which corresponds to minimum and maximum U_{ap}, and at $U_{ap} \approx U_\infty$. As explained before, vertical variation of U_{ap} exists for a rotor undergoing a pendulum motion. At the maximum U_{ap} the local velocity is highest at the bottom and lowest at the top along the turbine plane and *vice versa* for minimum U_{ap}, where the local velocity is highest at the top and lowest at the bottom along the turbine plane. These results correspond to the result presented in Figure 4b, where blade 1 has the lowest loading at both minimum and maximum U_{ap}, which happen because blade 1 is at azimuth angles of 0° and 180° at maximum and minimum U_{ap}, respectively. At the maximum U_{ap} flow separation occurs along blades 2 and 3 where there is a change in characteristics of the force profiles. This happens due to the high angle of attack on rotor blades at high U_{ap}.

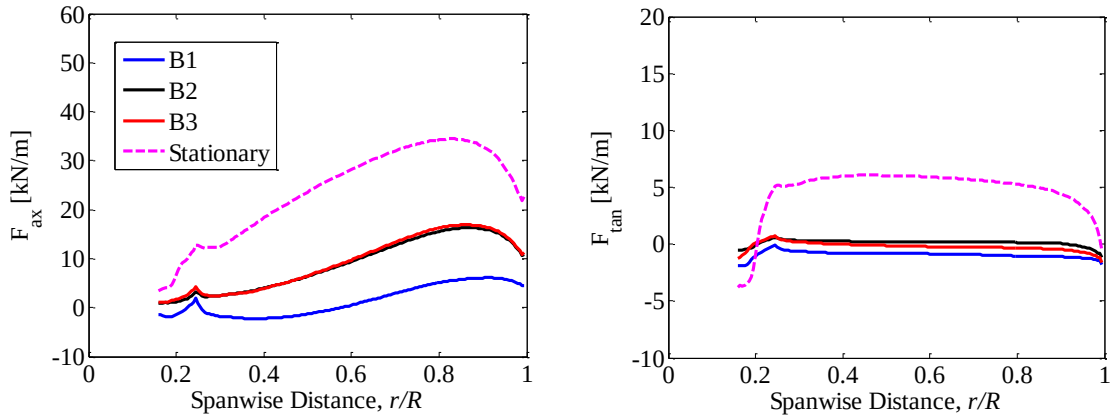

(a) minimum U_{ap}

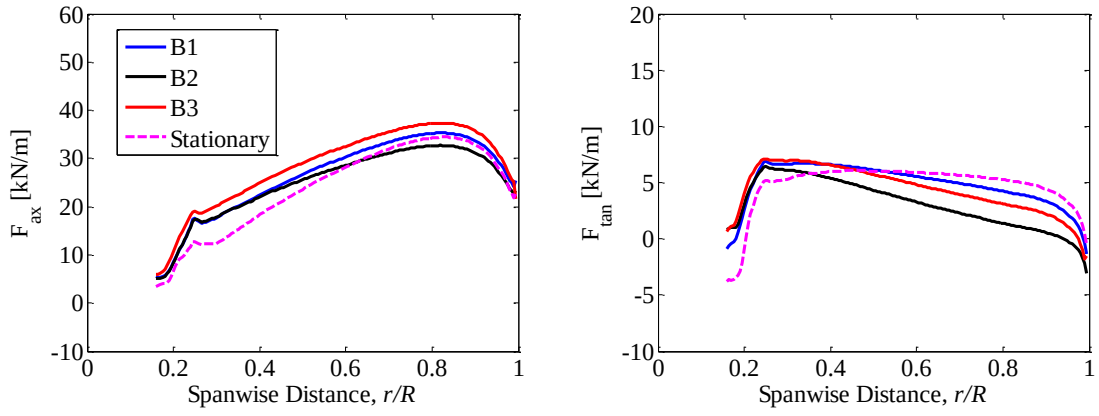

(b) $U_{ap} \approx U_{\infty}$

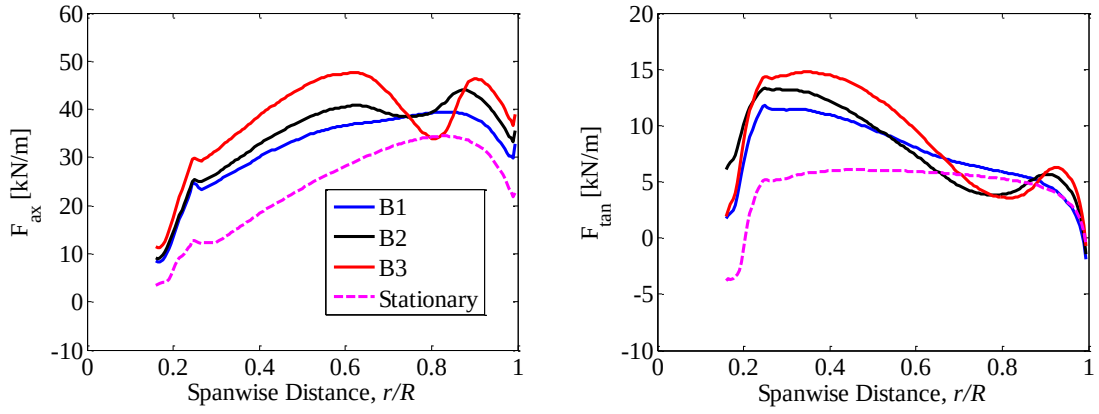

(c) maximum U_{ap}

Figure 6 Force profiles for all blades at different apparent velocity conditions at A_0 = 3.0° with a constant ω^* = 1.0 and λ = 4.2.

Flow visualisations are given in Figure 9a showing the difference in the instantaneous velocity magnitude between blades 1 and 3 at maximum U_{ap}. Although not presented here, this phenomenon (i.e., flow separation) does not occur at $A_0 \leq$ 1.5°. Comparison of pressure

coefficients between the case of $A_0 = 1.5°$ and 3° is presented in Figure 10 in the appendix showing the occurrence of flow separation in higher pendulum motion case.

5. Minimizing the stalling effect on an oscillating turbine

A rotor undergoing a pendulum motion at A_0 = 3.0° and ω^* = 1.0 was simulated using three different rotor rotational speeds ω_r = 0.76, 0.84, 0.92, and the power and thrust coefficients time histories for all three cases are presented in Figure 7.

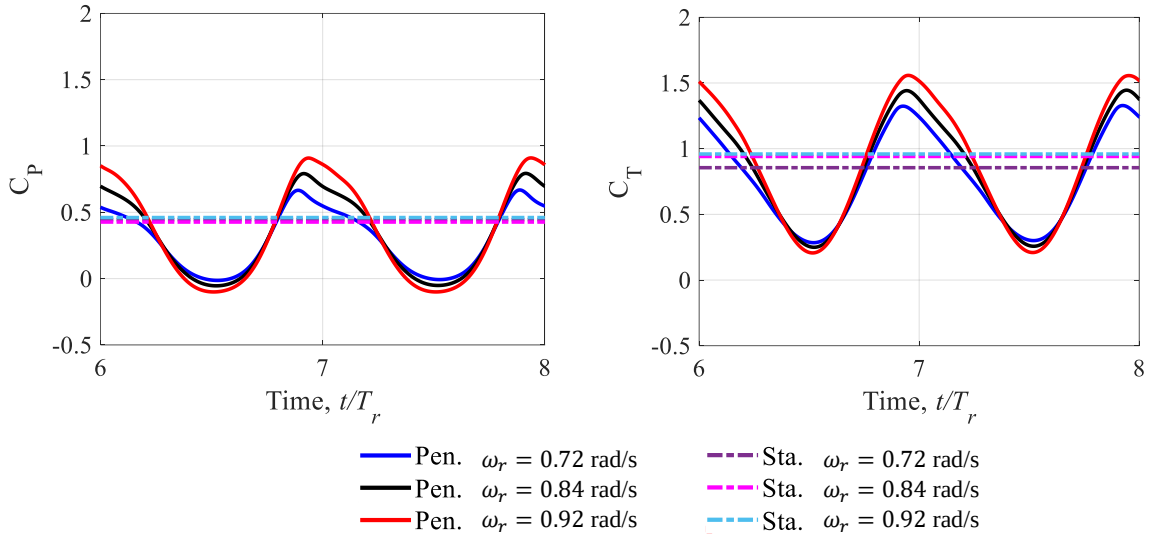

Figure 7 Power and thrust coefficients for a stationary (Sta.) and floating turbine undergoing a prescribed pendulum motion (Pen.) over a range of rotor rotational speed with A_0 = 3.0° and ω^* = 1.0.

These are typical results for a floating turbine undergoing a prescribed motion, where the amplitude of variation increases as the rotor rotational speed is increased (Wen et al., 2017; Jing et al., 2017; Sun et al., 2017). At the peak of each cycle, where the apparent velocity is at the maximum, the stalling effect is minimized as the rotor spins faster. For a floating turbine operating at a constant rotational speed, the instantaneous tip speed ratio will vary when it oscillates in the pendulum motion. For a stationary turbine, the tip speed ratio is inversely proportional to the free stream velocity. For a floating turbine, the instantaneous tip speed ratio calculation does not depend on the free stream velocity; rather, it depends on the rotor's instantaneous velocity (i.e., the apparent velocity). Hence, the instantaneous tip speed ratio λ_{in} for a floating turbine operating under a fixed rotational speed can be defined as

$$\lambda_{\text{in}}(t) = \frac{R\omega_r}{U_{ap}(t)} \qquad (7)$$

Therefore, at maximum $U_{ap}(t)$ the instantaneous tip speed ratio is not 4.2, but lower than that, and the opposite happens at the minimum $U_{ap}(t)$. So, operating a turbine at a higher than optimal rotational speed will make the rotor operates at near optimum instantaneous tip speed ratio when the apparent velocity goes to the maximum, thus minimizing the flow separation on each blade.

Since the stalling effect was minimized when operating a floating turbine at higher than optimal rotational speed, the rotor can extract more (average) power. Table 2 shows the percentage difference between floating and stationary turbines with their respective rotational speed. The rotor can extract more power relative to its rotational speed as the rotational speed increases. This happens due to the flow separation being minimized as the rotational speed is increased.

Table 2 Mean power and thrust coefficients for a floating turbine undergoing a prescribed pendulum motion at various rotational speeds with constant A_0 = 3.0° and ω^* = 1.0.

ω_r [rad/s]	$\bar{C}_P$	$\bar{C}_T$	Percentage difference $\bar{C}_P$ [%]	Percentage difference $\bar{C}_T$ [%]
Pendulum 0.72	0.303	0.791	33.502	10.903
Pendulum 0.84	0.344	0.853	25.711	6.975
Pendulum 0.92	0.371	0.909	19.403	5.245
Stationary 0.72	0.455	0.887	-	-
Stationary 0.84	0.463	0.917	-	-
Stationary 0.92	0.461	0.959	-	-

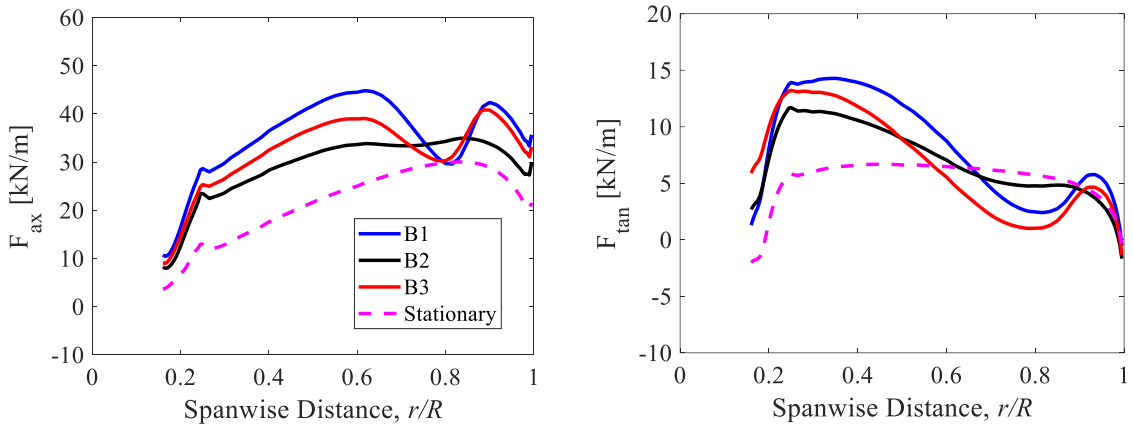

(a) ω_r = 0.76 rad/s at maximum U_{ap} ($\lambda = 3.8$)

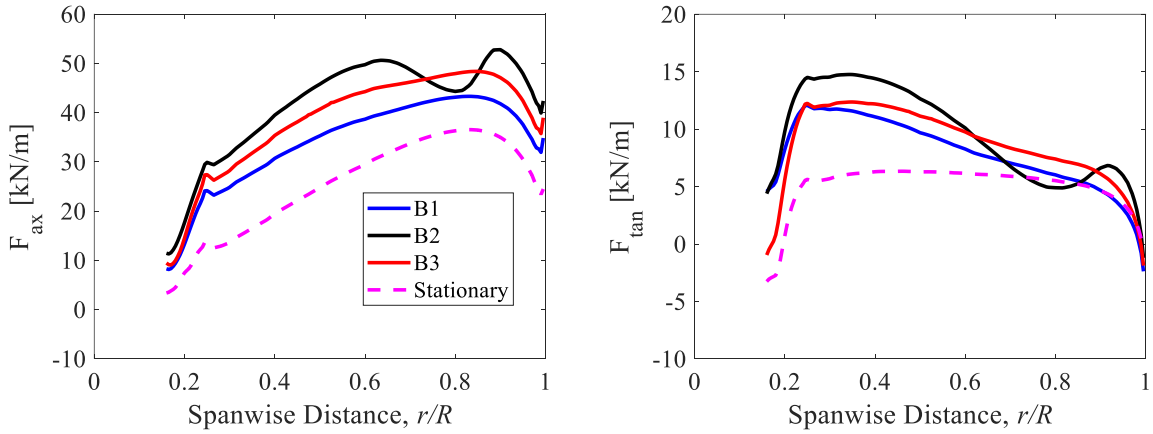

(b) ω_r = 0.92 rad/s at maximum U_{ap} ($\lambda = 4.6$)

Figure 8 Comparison of axial force profiles at maximum apparent velocity for each blade for a rotor operating at ω_r = 0.76 and 0.92 rad/s while undergoing a pendulum motion with A_0 = 3.0° and ω^* = 1.0.

When comparing the force profiles, given in Figure 8, on each blade for a floating turbine rotating at ω_r = 0.76 and 0.92 rad/s, at maximum U_{ap} the flow separation is minimized when rotating the rotor at a higher speed. This happens due to the operating tip speed ratio of the turbine. When the apparent velocity increase, the angle of attack will also increase. If the rotor spins at the optimum speed or lower, at maximum U_{ap} the rotor operates at a lower than optimum tip speed ratio condition, and flow separation on the blade surface will occur. If the rotor is rotating faster than the optimum speed, it will operate at a tip speed ratio closer to the optimum condition at high U_{ap} condition. Flow visualisation of the velocity magnitude for lower and higher rotational speed cases is given in Figure 9b in the appendix, showing flow separation is minimized as the rotational speed is increased.

6. Conclusion

To conclude, this paper investigates the hydrodynamic loading of a floating tidal turbine undergoing pendulum motion over a range of motion amplitude and frequency. As mentioned in the literature (Tran & Kim, 2015a; Leble & Barakos, 2016; Lienard et al., 2019), and the data presented here, the rotor loading variation is highly in phase with the apparent velocity. The typical result has been shown in the present study for the loading variation. The amplitude of variation increases as the motion amplitude is increased, and the mean power increases while the mean thrust decreases with the increase in motion amplitude. The overall mean power and thrust are significantly lower for the floating turbine compared to the stationary. This might be due to the rotor design used in the present study. Wimshurst & Willden (2016) optimized the blocked rotor design to operate in a high blockage condition (close to blockage ratio B = 20%). The present study uses B = 1%, which significantly affects the performance of the rotor when operating in an unsteady condition, such as oscillating in a pendulum motion. Loading variation for individual blades happens due to the vertical variation of the instantaneous apparent velocity, together with the azimuth angle of each blade at a given time step. The rotor goes into stall at higher motion amplitude and frequency cases due to the loss in lift along the rotor blades, particularly at higher apparent velocity because of the increase in the angle of attack. The floating tidal turbine undergoing pendulum motion operates near the optimum condition twice per motion cycle, where the rotor efficiency is at the maximum at $U_{ap} \approx U_{\infty}$.

The instantaneous tip speed ratio varies over time for a floating turbine due to the change in the apparent velocity of the rotor; a higher apparent velocity will reduce the instantaneous tip speed ratio and *vice versa* for a lower apparent velocity. Therefore, it is better to increase the speed of rotation (i.e., speed control technique) when operating a floating turbine at a high apparent velocity so that it will operate at an instantaneous tip speed ratio close to its optimum condition.

Acknowledgement

M. Osman thanks Majlis Amanah Rakyat Malaysia (MARA) and Universiti Teknologi Malaysia (UTM) for financial support, and Oxford University Advanced Research Computing (ARCUS) for providing high performance computing system services.

Authorship contribution statement

M. Osman: Methodology, data curation, visualization, investigation, writing – original draft.
R. Willden: Supervision, writing – review and editing.

APPENDIX

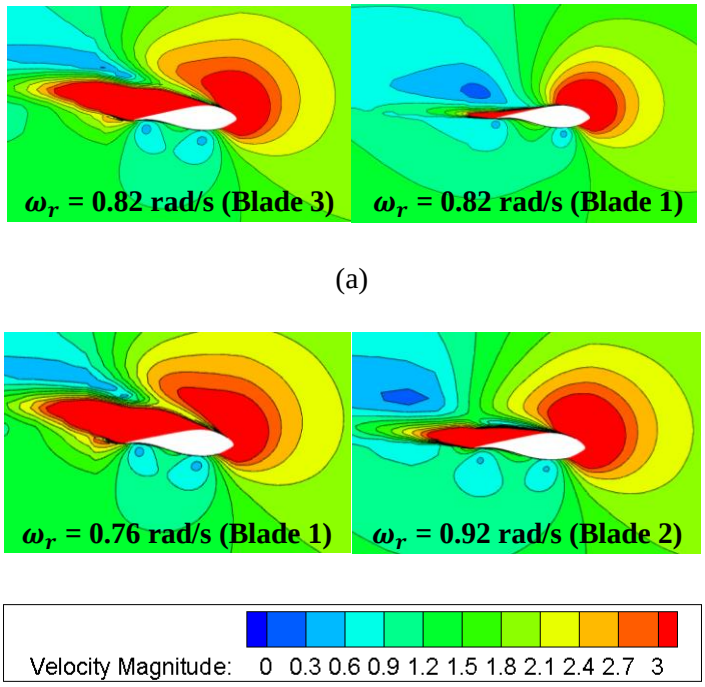

Figure 9 Cross-sections of velocity (magnitude) field contour plots for the case of A_0 = 3.0° and ω^* = 1.0 at spanwise distance *r/R* = 0.8 of: (a) blade 3 (left) and blade 1 (right) at maximum U_{ap} of a rotor undergoing a pendulum motion at λ = 4.2 (i.e., ω_r = 0.84 rad/s). Higher instantaneous velocity can be seen at blade 3 compared to blade 1, and the presence of swirling towards the trailing edge of blade 3 indicates flow separation; (b) ω_r = 0.76 and 0.92 rad/s at maximum U_{ap}, where swirling at the trailing edge is minimized at a higher rotational speed.

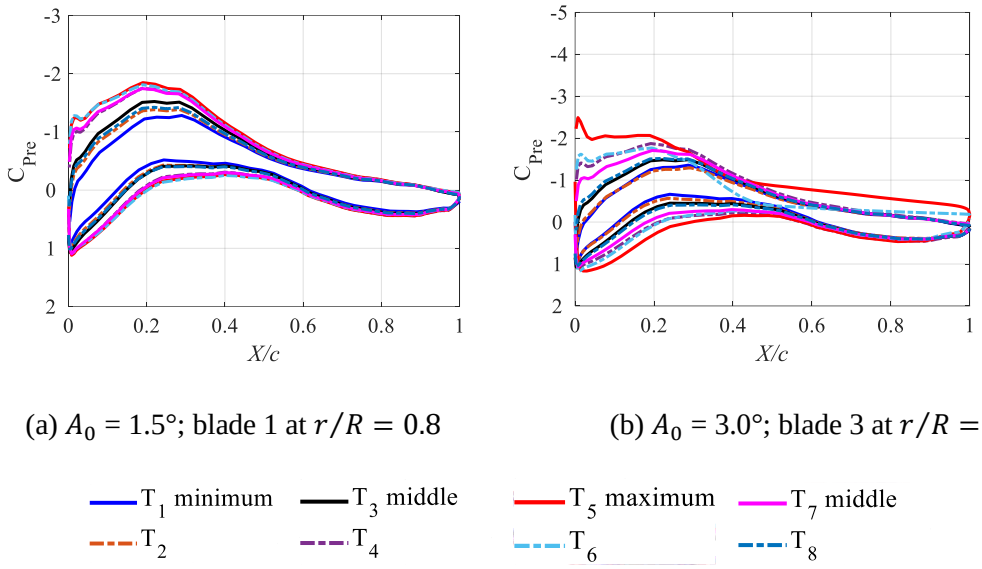

(a) A_0 = 1.5°; blade 1 at $r/R = 0.8$ (b) A_0 = 3.0°; blade 3 at $r/R = 0.8$

Figure 10 Pressure coefficients of a floating tidal turbine undergoing pendulum motion. The pressure coefficient in (b) at T_5 and T_6 plots show flat towards the trailing edge at the suction side, indicating flow separation occurs at that blade section.

References

Anatec Ltd. (2010). Navigation Risk Assessment Update Fall of Warness. *Technical Report*, *01*(A2343-EMEC-NRA-1).

Bagbanci, H. (2011). Dynamic Analysis of Offshore Floating Wind Turbines. *Centre for Marine Technology and Engineering (CENTEC), December*.

Brown, S. A., Ransley, E. J., & Greaves, D. M. (2020). Developing a coupled turbine thrust methodology for floating tidal stream concepts : Verification under prescribed motion. *Renewable Energy*, *147*, 529–540.

Brown, S. A., Ransley, E. J., Xie, N., Monk, K., Angelis, G. M. De, & Nicholls-lee, R. (2021). On the impact of motion-thrust coupling in floating tidal energy applications. *Applied Energy*, *282*(PB), 116246.

Brown, S. A., Ransley, E. J., Zheng, S., Xie, N., Howey, B., & Greaves, D. M. (2020). Development of a fully nonlinear, coupled numerical model for assessment of floating tidal stream concepts. *Ocean Engineering*, *218*(February), 108253.

Burton, T., Sharpe, D., Jenkins, N., & Bossanyi, E. (2001). *Wind energy handbook*. Jon

399 Wiley & Sons, Ltd.

400 Castro-Santos, L., & Diaz-Casas, V. (2015). Sensitivity analysis of floating offshore wind
401 farms. *Energy Conversion and Management*, *101*, 271–277.

402 Jing, F., Wang, S. qi, Sheng, Q. hu, Ma, Y., & Zhang, L. (2017). The effects of surge motion
403 of the floating platform on hydrodynamics performance of horizontal-axis tidal current
404 turbine. *Journal of Marine Science and Technology (Japan)*, *22*(2), 259–269.

405 Jonkman, J. M. (2009). Dynamics of offshore floating wind turbines-model development and
406 verification. *Wind Energy*, *12*(5), 459–492.

407 Leble, V., & Barakos, G. (2016). Forced pitch motion of wind turbines. *Journal of Physics:*
408 *Conference Series*, *753*(2).

409 Lienard, C., Boisard, R., & Daudin, C. (2019). Aerodynamic behavior of a floating offshore
410 wind turbine. *AIAA Scitech*.

411 Menter, F. R. (1994). Two-equation eddy-viscosity turbulence models for engineering
412 applications. *AIAA Journal*, *32*(8), 1598–1605.

413 Micallef, D., & Sant, T. (2015). Loading effects on floating offshore horizontal axis wind
414 turbines insurge motion. *Renewable Energy*, *83*, 737–748.

415 Osman, M. H. B., & Willden, R. H. J. (2021). Unsteady loading of a floating tidal turbine
416 oscillating in a pendulum motion. *Developments in Renewable Energies Offshore*, 571–
417 581.

418 Osman, M., Willden, R. H. J., & Vogel, C. R. (2020). The effects of surge motion on floating
419 horizontal axis tidal turbines. *International Marine Energy Journal*, *3*(2), 45–54.

420 Pegalajar-Jurado, A., Hansen, A. M., Laugesen, R., Mikkelsen, R. F., Borg, M., Kim, T.,
421 Heilskov, N. F., & Bredmose, H. (2016). Experimental and numerical study of a 10MW
422 TLP wind turbine in waves and wind. *Journal of Physics: Conference Series*, *753*(9).

423 Rodrigues, S. F., Teixeira Pinto, R., Soleimanzadeh, M., Bosman, P. A. N., & Bauer, P.
424 (2015). Wake losses optimization of offshore wind farms with moveable floating wind
425 turbines. *Energy Conversion and Management*, *89*, 933–941.

426 Schluntz, J., & Willden, R. H. J. (2015). The effect of blockage on tidal turbine rotor design
427 and performance. *Renewable Energy*, *81*, 432–441.

Sebastian, T., & Lackner, M. (2012). Analysis of the induction and wake evolution of an offshore floating wind turbine. *Energies*, *5*(4), 968–1000.

Shen, X., Hu, P., Chen, J., Zhu, X., & Du, Z. (2018). The unsteady aerodynamics of floating wind turbine under platform pitch motion. *Proceedings of the Institution of Mechanical Engineers, Part A: Journal of Power and Energy*, *232*(8), 1019–1036.

SIMEC Atlantis Energy. (2016). AR1500 tidal turbine. *Technical Report*, 1–6. https://www.atlantisresourcesltd.com/wp/wp-content/uploads/2016/08/AR1500-Brochure-Final-1.pdf

Sun, K., Zhang, J. hua, Zhang, L., & Wang, S. qi. (2017). The effects of roll motion of the floating platform on hydrodynamics performance of horizontal-axis tidal current turbine. *Journal of Marine Science and Technology (Japan)*, *22*(2), 259–269.

Tran, T., Kim, D., & Song, J. (2014). Computational fluid dynamic analysis of a floating offshore wind turbine experiencing platform pitching motion. *Energies*, *7*(8), 5011–5026.

Tran, T. T., & Kim, D. H. (2015a). The aerodynamic interference effects of a floating offshore wind turbine experiencing platform pitching and yawing motions. *Journal of Mechanical Science and Technology*, *29*(2), 549–561.

Tran, T. T., & Kim, D. H. (2015b). The platform pitching motion of floating offshore wind turbine: A preliminary unsteady aerodynamic analysis. *Journal of Wind Engineering and Industrial Aerodynamics*, *142*, 65–81.

Wen, B., Tian, X., Dong, X., Peng, Z., & Zhang, W. (2017). Influences of surge motion on the power and thrust characteristics of an offshore floating wind turbine. *Energy*, *141*, 2054–2068.

Wen, B., Tian, X., Zhang, Q., Dong, X., Peng, Z., Zhang, W., & Wei, K. (2019). Wind shear effect induced by the platform pitch motion of a spar-type floating wind turbine. *Renewable Energy*, *135*, 1186–1199.

Wimshurst, A., & Willden, R. (2016). *Computational analysis of blockage designed tidal turbine rotors*. *Progress in Renewable Energies Offshore*, 587–600.

Xie, N., Ransley, E. J., Brown, S., Greaves, D., Nicholls-Lee, R., Johanning, L., Weston, P., & Guerrini, E. (2019). Wave tank experiments of a floating, tidal-stream energy device.

458 *Advances in Renewable Energies Offshore - Proceedings of the 3rd International*
459 *Conference on Renewable Energies Offshore, RENEW 2018*, *October*, 203–207.

460